Production cross sections of dysprosium, terbium and gadolinium radioisotopes from the alpha-particle-induced reactions on natural gadolinium up to 50 MeV

Dagvadorj Ichinkhorloo[1,2*], Masayuki Aikawa[1,3], Zolbadral Tsoodol[2,3], Tomohiro Murata[3], Michiya Sakaguchi[3], Yukiko Komori[4], Takuya Yokokita[4], Hiromitsu Haba[4]

[1] *Faculty of Science, Hokkaido University, Sapporo 060-0810, Japan*

[2] *Nuclear Research Center, National University of Mongolia, Ulaanbaatar 13330, Mongolia*

[3] *Graduate School of Biomedical Science and Engineering, Hokkaido University, Sapporo 060-8638, Japan*

[4]*Nishina Center for Accelerator-Based Science, RIKEN, Wako 351-0198, Japan*

Abstract

The activation cross sections of the alpha-particle-induced reactions on natural gadolinium up to 50 MeV were measured. The stacked foil technique, the activation method and the γ-ray spectrometry were used for the measurement. We determined the experimental production cross sections of ^{155,157,159}Dy, ^{153,155,156g,160,161}Tb and ^{153}Gd. No previous experimental data of ^{155,159}Dy, and ^{153}Gd were found in the literature. The measured values were compared with the previous experimental data and the TENDL-2019 data.

Keyword

Dysprosium-157; Dysprosium-159; Terbium-155; Alpha irradiation; Gadolinium target; Excitation function; Cross section

1. Introduction

Dysprosium and terbium radioisotopes are of interest for diagnosis and therapy in nuclear medicine. Dysprosium-157 ($T_{1/2}$ = 8.14 h), dysprosium-159 ($T_{1/2}$ = 144.4 d), and terbium-155 ($T_{1/2}$ = 5.32 d) can be used for bone scanning (Skeletal imaging) [1], determination of bone mineral [2] and SPECT imaging [3], respectively. We studied the production cross sections of ^{157,159}Dy in the deuteron-induced reactions on ^{159}Tb [4]. These radionuclides can also be produced by alpha-particle-induced reactions on enriched and natural gadolinium [5–8]. Among them, we focused on the reaction on natural gadolinium, of which isotopic composition is ^{152}Gd (0.20%), ^{154}Gd (2.18%), ^{155}Gd (14.79%), ^{156}Gd (20.47%), ^{157}Gd (15.65%), ^{158}Gd (24.83%), and ^{160}Gd (21.86%). In this work, the activation cross sections of the alpha-particle-induced reactions on natural gadolinium were studied. The production cross sections of ^{155,157,159}Dy, ^{153,155,156g,160,161}Tb and ^{153}Gd were determined. The results were

* Corresponding author: ichinkhorloo@nucl.sci.hokudai.ac.jp

compared with the experimental data studied earlier [5,6] and the TENDL-2019 data based on calculation using the TALYS code [9].

2. Experimental

The experiment was performed at the RIKEN AVF cyclotron. In the experiment, we used the stacked foil technique, the activation method, and high-resolution γ-ray spectrometry to determine the activation cross sections.

The stacked target consisted of ^{nat}Gd and ^{nat}Ti foils. The thicknesses of the ^{nat}Gd (50 × 50 mm, 99.9% purity, Nilaco Corp., Japan) and ^{nat}Ti foils (50 × 100 mm, 99.6% purity, Nilaco Corp., Japan) were 25.4 and 2.25 mg/cm^2, respectively, which were derived from their measured weight and lateral size. The foils were cut into 8 × 8 mm to fit a target holder serving as a Faraday cup. Fourteen sets of Gd-Ti-Ti foils were stacked as the target. To handle the recoil effect, for monitoring the alpha-particle beam, using the ^{nat}Ti(α,x)^{51}Cr monitor reaction, every second Ti foil from the Ti-Ti pairs was used.

The stacked target was irradiated with an alpha-particle beam for 60 min. The beam was accelerated to 51.0±0.1 MeV by the RIKEN AVF cyclotron. The beam energy was measured using the time-of-flight method [10]. Energy degradation in the stacked target was calculated using the SRIM code [11]. The average beam intensity of 258 nA was measured using the Faraday cup.

The γ rays emitted from the irradiated foils were measured by a high-resolution HPGe detector (ORTEC GEM30P4-70). The detector was calibrated by using a standard γ-ray source composed of ^{57,60}Co, ^{88}Y, ^{109}Cd, ^{113}Sn ^{137}Cs, ^{139}Ce and ^{241}Am. The γ-ray spectra were analyzed by using the software Gamma Studio (SEIKO EG&G). The γ-ray spectra of each foil were measured four times after cooling times at different distances (14.3-17.6 h at 2 and 75 cm, 1.4-1.7 d at 2, 10 and 25 cm, 2.4-2.8 d at 2 and 10 cm, 25.4-28.8 d at 2 and 5 cm). The dead time of the measurements was kept below 6.3%. Reaction and decay data for the γ-ray spectrometry were taken from NuDat 2.8 [12], Lund/LBNL Nuclear Data Search [13], LiveChart [14] and QCalc [15] and summarized in Table 1.

Table 1. Reactions and decay data of reaction products [12–15]

Nuclide	Half-life	Decay mode (%)	E_γ (keV)	I_γ (%)	Contributing reactions	Q-value (MeV)
^{155}Dy	9.9 h	ε+β$^+$ (100)	184.564	3.39(8)	^{152}Gd(α,n)	-11.2
			226.918	68.7(16)	^{154}Gd(α,3n)	-26.3
					^{155}Gd(α,4n)	-32.8
					^{156}Gd(α,5n)	-41.3
					^{157}Gd(α,6n)	-47.7
^{157}Dy	8.14 h	ε+β$^+$ (100)	182.424	1.33(6)	^{154}Gd(α,n)	-9.9
			326.336	93(3)	^{155}Gd(α,2n)	-16.4
					^{156}Gd(α,3n)	-24.9

					^{157}Gd(α,4n)	-31.3
					^{158}Gd(α,5n)	-39.2
^{159}Dy	144.4 d	ε (100)	**58.0**	2.27(13)	^{155}Gd(α,γ)	-0.5
					^{156}Gd(α,n)	-9.0
					^{157}Gd(α,2n)	-15.4
					^{158}Gd(α,3n)	-23.3
					^{160}Gd(α,5n)	-36.7
^{153}Tb	2.34 d	ε+β^+ (100)	82.86	5.4(7)	^{152}Gd(α,t)	-15.9
			102.255	5.8(5)	^{154}Gd(α,2nt)	-31.1
			109.758	6.2(4)	^{155}Gd(α,3nt)	-37.5
			170.42	5.8(4)	^{156}Gd(α,4nt)	-46.0
			212.00	31.0(18)	^{153}Dy(ε)	
^{155}Tb	5.32 d	ε (100)	86.55	32.0(18)	^{152}Gd(α,p)	-8.3
			105.318	25.1(13)	^{154}Gd(α,t)	-15.0
			148.64	2.65(14)	^{155}Gd(α,nt)	-21.4
			161.29	2.76(15)	^{156}Gd(α,2nt)	-30.0
			163.28	4.44(23)	^{157}Gd(α,3nt)	-36.3
			180.08	7.5(4)	^{158}Gd(α,4nt)	-44.3
			262.27	5.3(3)	^{155}Dy(ε)	
^{156g}Tb	5.35 d	ε+β^+ (100)	199.19	41(5)	^{154}Gd(α,d)	-14.3
			262.54	5.8(6)	^{155}Gd(α,t)	-14.5
			296.49	4.5(4)	^{156}Gd(α,nt)	-23.0
			356.38	13.6(13)	^{157}Gd(α,2nt)	-29.4
			422.34	8.0(8)	^{158}Gd(α,3nt)	-37.3
			534.29	67(6)		
			1065.11	10.8(10)		
			1154.07	10.4(10)		
			1222.44	31(3)		
^{160}Tb	72.3 d	β^- (100)	86.7877	13.2(3)	^{157}Gd(α,p)	-7.9
			298.5783	26.1(6)	^{158}Gd(α,d)	-13.6
			879.378	30.1(6)	^{160}Gd(α,nt)	-20.7
			966.166	25.1(5)		
			1177.954	14.9(3)		
^{161}Tb	6.89 d	β^- (100)	**74.56669**	10.2(5)	^{158}Gd(α,p)	-8.1
			87.941	0.183(10)	^{160}Gd(α,t)	-13.0
			103.065	0.101(6)	^{161}Gd(β^-)	

^{153}Gd	240.4 d	ε (100)	69.673	2.45(7)	^{152}Gd(α,^{3}He)	-14.3
			97.431	29.0(8)	^{154}Gd(α,nα)	-8.9
			103.1801	22.1(3)	^{155}Gd(α,2nα)	-15.3
					^{156}Gd(α,3nα)	-23.9
					^{157}Gd(α,4nα)	-30.2
					^{158}Gd(α,5nα)	-38.2
					^{153}Tb(ε)	

The self-absorption of low energy γ rays in the ^{nat}Gd foils were corrected using the following formula [16]

$$A(E) = A_0(E)\frac{\rho[\mu(E)/\rho]d}{1-\exp\left[-\rho(\mu(E)/\rho)d\right]}, \quad (1)$$

where $A_0(E)$ is the measured activity for the γ ray at the energy E, $A(E)$ is the corrected activity, d is the thickness of the ^{nat}Gd foil, ρ is the density of the foil, $\mu(E)/\rho$ is the mass attenuation coefficient for the γ ray at the energy E taken from [17].

3. Result and discussion

The cross sections of the ^{nat}Ti(α,x)^{51}Cr monitor reaction were derived using the γ-ray line at 320.1 keV (I_γ = 9.91%). The derived cross sections were compared with the recommended values from IAEA [18]. Based on the comparison, an energy shift toward the lower energy was found. Therefore, the measured target thickness of the ^{nat}Gd foil was corrected within its uncertainty by decreasing 3%. The corrected cross sections of the monitor reaction are shown in Fig. 1. We could obtain a good agreement between our experimental result and the recommended values. The measured thickness of the ^{nat}Ti foil and beam intensity were adopted for the following analysis.

Production cross sections of ^{155,157,159}Dy, ^{153,155,156g,160,161}Tb and ^{153}Gd in the alpha-particle-induced reactions on ^{nat}Gd were determined. The numerical data are tabulated in Table 2 and graphically shown in Figs. 2-10 in comparison with the previous experimental data [5,6] and the TENDL-2019 data [9]. The total uncertainties (8.6-29.3%) were estimated from the square root of the quadratic summation of each component; statistical uncertainty (0.02-27.7%), target thickness (3%), target purity (1%), beam intensity (5%), detector efficiency (6%), and γ-ray intensity (3-18%).

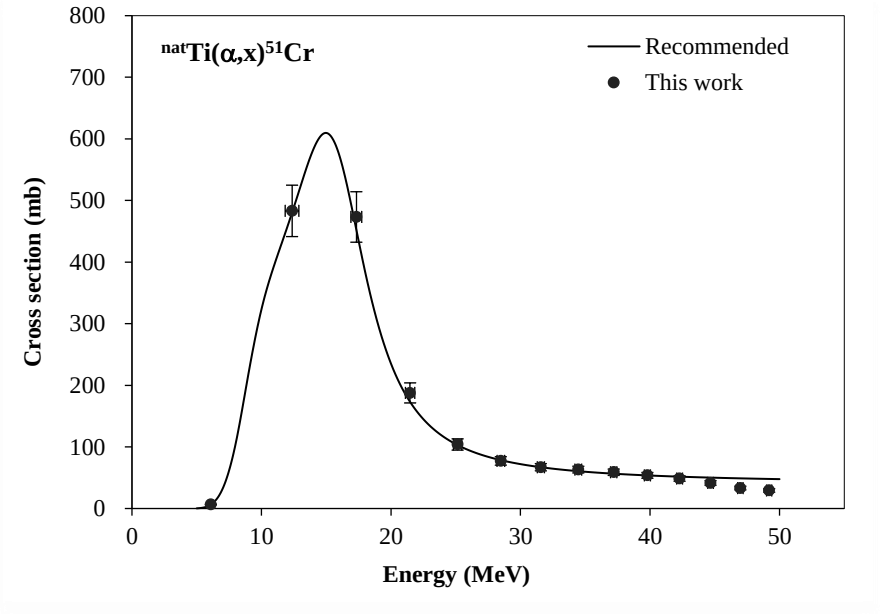

Fig. 1. Excitation function of the ^{nat}Ti(α,x)^{51}Cr monitor reaction with the recommended values [18].

Table 2. Production cross sections obtained in the experiment

Energy (MeV)	^{155}Dy (mb)	^{157}Dy (mb)	^{159}Dy (mb)	^{153}Tb (mb)	^{155}Tb (mb)	^{156g}Tb (mb)	^{160}Tb (mb)	^{161}Tb (mb)	^{153}Gd (mb)
50.3±0.9	233±20	367±32	300±32	2.25±0.25	234±23	24.0±3.0	18.9±1.7	18.0±1.9	10.6±1.1
48.1±0.9	205±18	342±30	248±26	2.03±0.22	209±21	19.7±2.5	15.6±1.4	17.8±1.8	9.39±0.94
45.8±0.9	183±16	351±30	212±22	2.61±0.28	189±19	16.2±2.0	13.0±1.2	18.9±1.9	9.75±0.95
43.4±0.9	142±12	371±32	202±22	2.91±0.31	144±14	12.5±1.6	11.5±1.0	16.5±1.7	7.61±0.77
41.0±1.0	80.7±7.0	355±31	203±21	2.53±0.27	75.9±7.6	6.98±0.86	8.77±0.79	12.5±1.2	5.75±0.54
38.5±1.0	42.6±3.7	343±30	279±29	2.21±0.24	39.9±4.0	4.86±0.61	7.67±0.69	10.1±1.0	3.24±0.32
35.8±1.1	25.6±2.3	324±28	350±36	1.54±0.17	24.3±2.5	3.22±0.41	7.47±0.67	7.88±0.79	2.16±0.23
33.0±1.1	13.1±1.2	262±23	346±36	0.494±0.06	12.8±1.3	1.65±0.22	5.69±0.52	5.78±0.58	0.541±0.101
30.0±1.2	3.33±0.31	215±19	312±32	0.0608±0.011	2.91±0.31	0.907±0.129	3.63±0.34	4.16±0.42	
26.8±1.3		162±14	216±22		0.405±0.082	0.255±0.061	1.81±0.18	2.84±0.31	
23.3±1.4		115±10	134±14		0.738±0.108			1.09±0.15	
19.4±1.6		38.2±3.4	78.5±8.1		0.290±0.041			0.190±0.056	
14.8±1.9		0.352±0.031							

3.1 ^{nat}Gd(α,x)^{155}Dy reaction

The activation cross sections of the ^{nat}Gd(α,x)^{155}Dy reaction were measured for the first time as far as we know. The measurements of the γ-ray line at 226.9 keV (I_γ = 68.4 %) from the ^{155}Dy decay ($T_{1/2}$ =

9.9 h) after cooling times of 14.3-17.6 h were adopted. We could obtain the cross sections in the energy range from 30 to 50 MeV. Our result is compared with the TENDL-2019 data [9] as shown in Fig. 2. The TENDL-2019 data somewhat overestimates our data between 35 and 45 MeV.

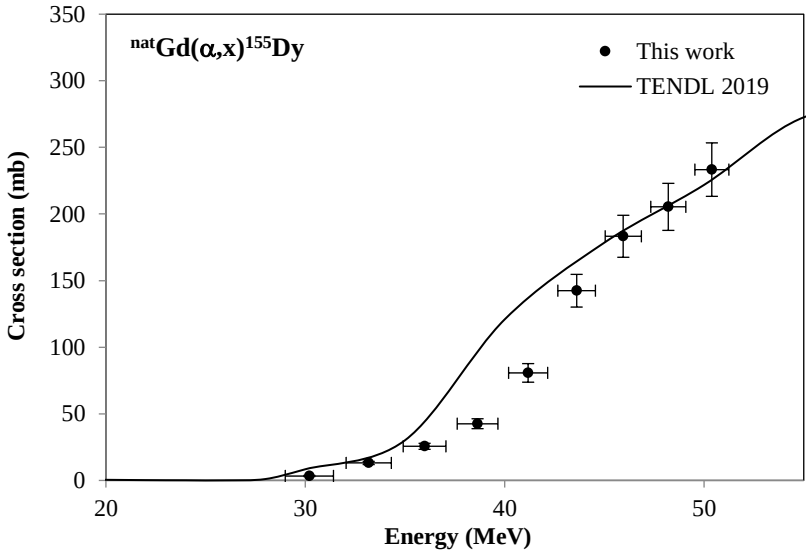

Fig. 2. Excitation function of the $^{nat}Gd(\alpha,x)^{155}Dy$ reaction

3.2 $^{nat}Gd(\alpha,x)^{157}Dy$ reaction

The excitation function of the $^{nat}Gd(\alpha,x)^{157}Dy$ reaction was determined based on the γ-ray line at 326.3 keV (I_γ = 93.0%) from the decay of ^{157}Dy ($T_{1/2}$ = 8.14 h). The measurements after cooling times of 14.3-17.6 h were used to derive the cross sections. We could obtain the cross sections in the energy range from 15 to 50 MeV. Our result is shown in Fig. 3 in comparison with the previous experimental study [6] and the TENDL-2019 data [9]. Our result is in good agreement with the experimental data. The TENDL-2019 data show two peaks contributed from the reactions on different Gd isotopes while ours monotonically increases up to 44 MeV. The TENDL-2019 data underestimate most of our experimental data above 25 MeV although they agree with ours below 25 MeV.

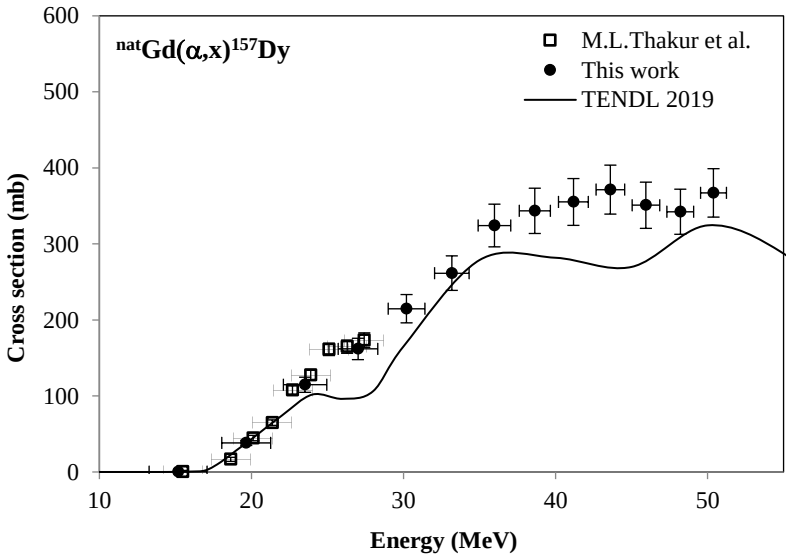

Fig. 3. Excitation function of the $^{nat}Gd(\alpha,x)^{157}Dy$ reaction

3.3 The $^{nat}Gd(\alpha,x)^{159}Dy$ reaction

The cross sections of the $^{nat}Gd(\alpha,x)^{159}Dy$ reaction were determined using the γ-ray line at 58.0 keV (I_γ = 2.27%) from the ^{159}Dy decay ($T_{1/2}$ = 144.4 d). To reduce γ-ray backgrounds from the short-lived radionuclides, the measurements were executed after cooling times of 25.4-28.8 d. The mass attenuation coefficient adopted for the γ-ray line at 58.0 keV was 12.8 cm^2/g [17]. The correction factor calculated from Eq. (1) is 1.17. The cross sections for the ^{159}Dy production derived from the corrected activities are presented with the TENDL-2019 data in Fig. 4. Our experimental data have peaks at around 35 and above 50 MeV. The peak amplitude and positions of the TENDL-2019 data agree with our data. There are no previous experimental data in our literature survey.

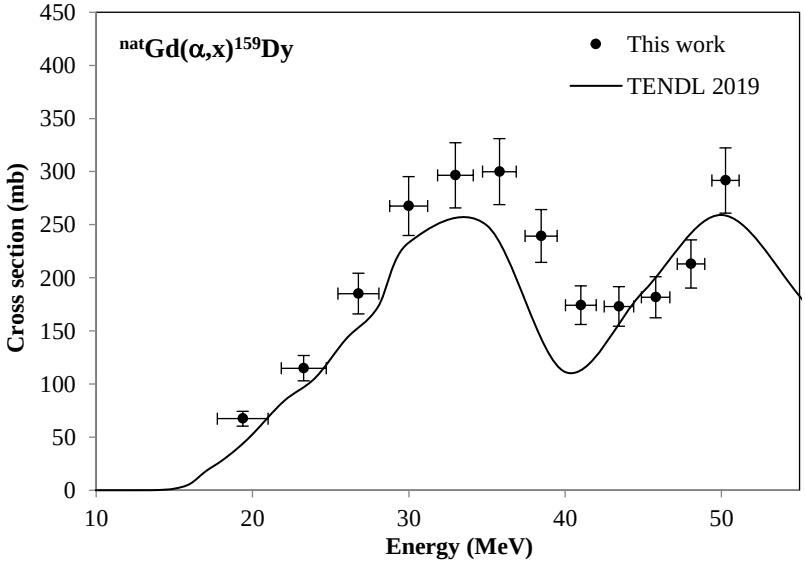

Fig. 4. Excitation function of the $^{nat}Gd(\alpha,x)^{159}Dy$ reaction

3.4 ^{nat}Gd(α,x)^{153}Tb reaction

The radionuclide ^{153}Tb has the half-life of $T_{1/2}$ = 2.34 d. The measurements of the 212.048-keV γ-ray line (I_γ = 31 %) from the ^{153}Tb decay were performed after cooling times of 2.4-2.8 d. The production of its parent ^{153}Dy ($T_{1/2}$ = 6.4 h) was energetically possible but not identified because no peaks of the specific γ-lines were found. The cumulative cross sections of the ^{nat}Gd(α,x)^{153}Tb reaction are shown in Fig. 5 together with the experimental data by Gayoso et al. [5] and the TENDL-2019 data [9]. Our experimental result has a peak around 44 MeV, which is different from the data of Gayoso et al. The TENDL-2019 data are very different from the two experimental data.

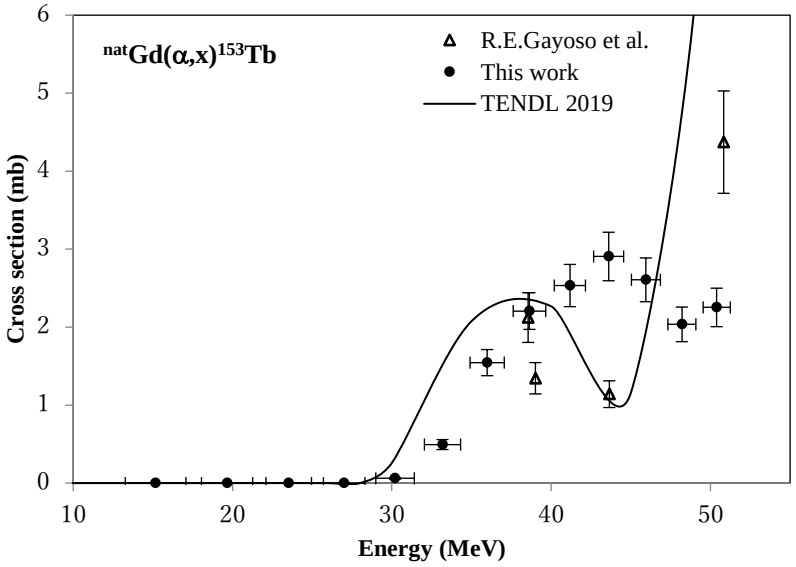

Fig. 5. Excitation function of the ^{nat}Gd(α,x)^{153}Tb reaction

3.5 ^{nat}Gd(α,x)^{155}Tb reaction

The γ-ray line at 105.3 keV (I_γ = 25.1%) emitted with the ^{155}Tb decay ($T_{1/2}$ = 5.32 d) was measured to derive the cross sections of the ^{nat}Gd(α,x)^{155}Tb reaction after cooling times of 25.4-28.8 d. The cooling time is long enough for the complete decay of the parent nuclide ^{155}Dy ($T_{1/2}$ = 9.9 h). The mass attenuation coefficient adopted for the γ-ray line is 2.74 cm^2/g [17] and the calculated correction factor from Eq. (1) is 1.03. The corrected cross sections are presented in Fig. 6 with those in the earlier study [5] and the TENDL-2019 data [9]. Our result shows acceptable agreement with the TENDL-2019 data except the middle energy region of 35–45 MeV. The previous experimental data are smaller than ours above 40 MeV.

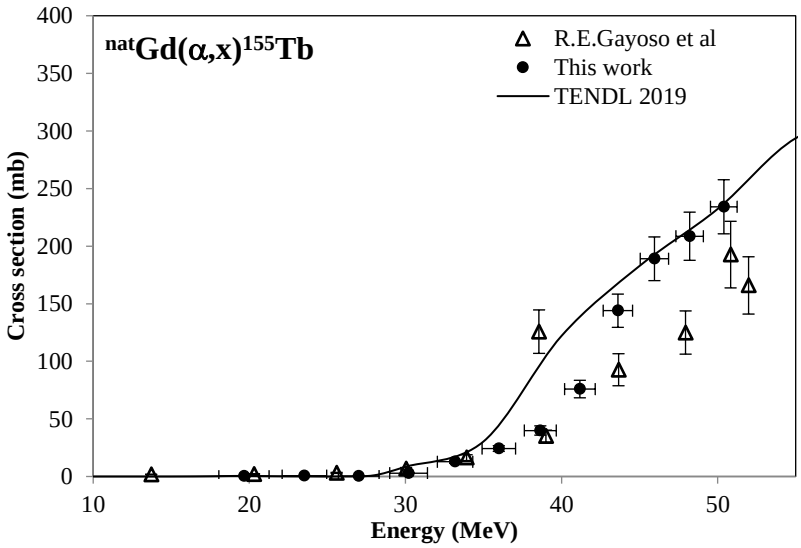

Fig. 6. Excitation function of the $^{nat}Gd(\alpha,x)^{155}Tb$ reaction

3.6 $^{nat}Gd(\alpha,x)^{156g}Tb$ reaction

The production cross sections of ^{156g}Tb ($T_{1/2}$ = 5.35 d) are shown in Fig.7. The measurement of 534.29-keV γ-ray line (I_γ = 67 %) from the ^{156g}Tb decay after cooling times of 25.4-28.8 d was adopted to derive the cross sections. The γ-ray lines from the two isomers at level energy of 0.0496 ($T_{1/2}$ = 24.4 h) and 0.0884 MeV ($T_{1/2}$ = 5.3 h) could not be identified in the spectra. During the cooling times, the isomers decayed to ^{156g}Tb, and thus the derived cross sections of ^{156g}Tb were cumulative. Our results show a good agreement with the experimental data by Gayoso et al. [5] and the TENDL-2019 data in the energy region.

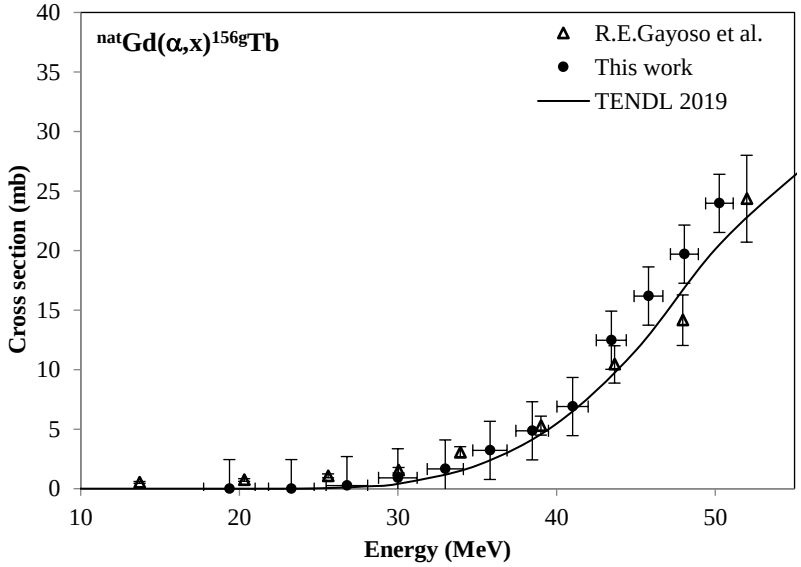

Fig. 7. Excitation function of the $^{nat}Gd(\alpha,x)^{156g}Tb$ reaction

3.7 ^{nat}Gd(α,x)^{160}Tb reaction

The radionuclide ^{160}Tb has the half-life of $T_{1/2}$ = 72.3 d. The measurements of the 879.301-keV γ-ray line (I_γ = 30.1 %) from the ^{160}Tb decay were used to derive the production cross sections after cooling times of 25.4-28.8 d. The derived cross sections are shown in Fig. 8 together with one experimental dataset by Gayoso et al. [5] and the TENDL-2019 data [9]. Both are lower than our results.

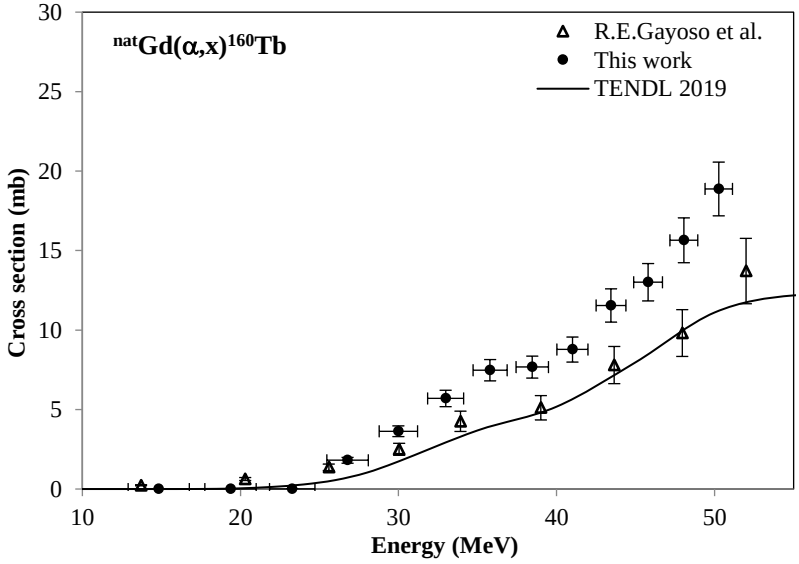

Fig. 8. Excitation function of the ^{nat}Gd(α,x)^{160}Tb reaction

3.8 ^{nat}Gd(α,x)^{161}Tb reaction

The excitation function of the ^{nat}Gd(α,x)^{161}Tb reaction was determined based on the γ-ray line at 74.56 keV (I_γ = 10.2%) from the decay of ^{161}Tb ($T_{1/2}$ = 6.89 d). The measurements after cooling times of 25.4-28.8 d were used to derive the cross sections. During the cooling time, the parent nuclide ^{161}Gd ($T_{1/2}$ = 3.66 min) decayed to ^{161}Tb. The correction factor calculated from Eq. (1) for the γ-ray line is 1.09 using the mass attenuation coefficient of 6.69 cm^2/g [17]. The cumulative cross sections using the corrected activities are compared with the data of Gayoso et al. [5] and the TENDL-2019 data [9] as shown in Fig. 9. Our data are higher than those of Gayoso et al. and the TENDL-2019 data by about a factor of two.

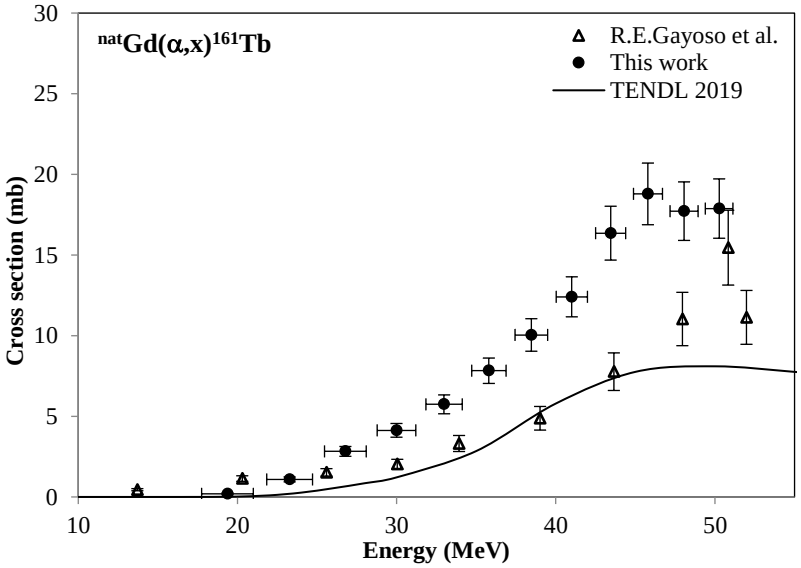

Fig. 9. Excitation function of the $^{nat}Gd(\alpha,x)^{161}Tb$ reaction

3.9 $^{nat}Gd(\alpha,x)^{153}Gd$ reaction

The production cross sections of ^{153}Gd ($T_{1/2}$= 240.4 d) using the γ-ray line at 97.431-keV (I_γ = 29%) are shown in Fig.10. The co-produced ^{153}Dy and ^{153}Tb decayed to ^{153}Gd during cooling times of 25.4-28.8 d. The activities were corrected by the correction factor of 1.04 calculated from Eq. (1) and the mass attenuation coefficient of 3.35 cm^2/g [17]. Cumulative cross sections were derived from the corrected activities. We compared our result with the TENDL-2019 data [9]. The TENDL-2019 data are slightly larger than ours. No experimental data studied earlier for the reaction were found in our survey.

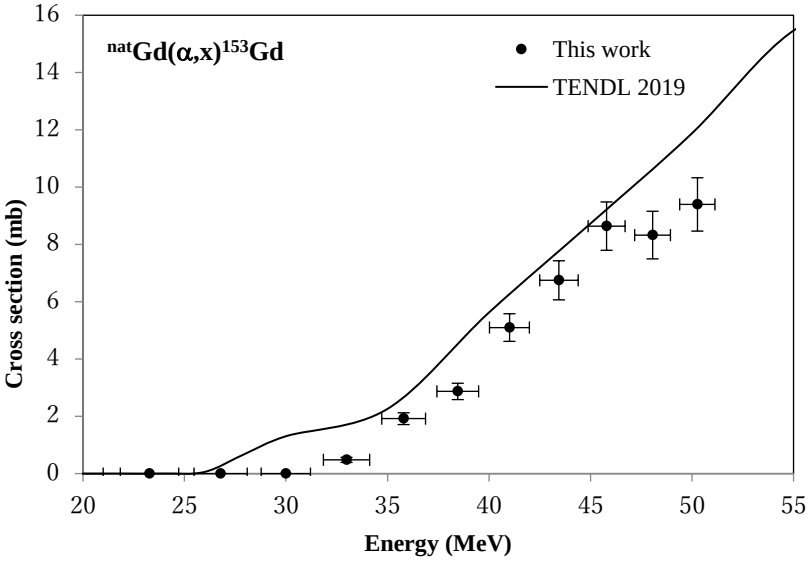

Fig. 10. Excitation function of the $^{nat}Gd(\alpha,x)^{153}Gd$ reaction

4. Summary

We investigated the production cross sections of ^{155,157,159}Dy and ^{153,155,156g,160,161}Tb and ^{153}Gd in the alpha-particle-induced reactions on ^{nat}Gd up to 50 MeV at the RIKEN AVF cyclotron. The cross sections of ^{155,159}Dy, and ^{153}Gd were measured for the first time. The stacked foil technique, the activation method and the high-resolution γ-ray spectrometry were used. The results were compared with the previous experimental data [5,6] and the TENDL-2019 data based on calculation using the theoretical model code TALYS [9]. We found that our data agree with the result of Thakur et al. but data of Gayoso et al. in most of the cases are lower than our results, which systematic deviation can be explained with a systematic error in their experiment. The TALYS calculation provided more or less the same shape for the investigated excitation functions with some differences in the structure and the amplitude of the curves.

Acknowledgement

This work was carried out at RI Beam Factory operated by RIKEN Nishina Center and CNS, University of Tokyo, Japan. This work was supported by JSPS KAKENHI Grant Number 17K07004.

Declarations of interest

None

References

[1] G. Subramanian, J.G. McAfee, R.J. Blair, R.E. O'Mara, M.W. Greene, E. Lebowitz, ^{157}Dy-HEDTA for skeletal imaging., J. Nucl. Med. 12 (1971) 558–61.

[2] D. V. Rao, G.F. Govelitz, K.S.R. Sastry, Dysprosium 159 for transmission imaging and bone mineral analysis, Med. Phys. 4 (1977) 109–114. https://doi.org/10.1118/1.594307.

[3] C. Muller, K. Zhernosekov, U. Koster, K. Johnston, H. Dorrer, A. Hohn, N.T. van der Walt, A. Turler, R. Schibli, A Unique Matched Quadruplet of Terbium Radioisotopes for PET and SPECT and for and Radionuclide Therapy: An In Vivo Proof-of-Concept Study with a New Receptor-Targeted Folate Derivative, J. Nucl. Med. 53 (2012) 1951–1959. https://doi.org/10.2967/jnumed.112.107540.

[4] D.Ichinkhorloo, M.Aikawa, Z.Tsoodol, Y.Komori, H.Haba, Activation cross sections of dysprosium-157,159 and terbium-160 radioisotopes from the deuteron-induced reactions on terbium-159 up to 24 MeV, Nucl. Instruments Methods Phys. Res. Sect. B Beam Interact. with Mater. Atoms. 461 (2019) 102–104. https://doi.org/10.1016/j.nimb.2019.09.037.

[5] R.E.Gayoso, A.A.Sonzogni, S.J. Nassiff, (α,pxn) Reactions on Natural Gadolinium, Radiochim. Acta. 72 (1996) 55–60. https://doi.org/10.1524/ract.1996.72.2.55.

[6] M.L.Thakur, S.L.Waters, Production and separation of cyclotron produced dysprosium-157, J.

Inorg. Nucl. Chem. 35 (1973) 1787–1791. https://doi.org/10.1016/0022-1902(73)80112-5.

[7] D. Chmielewska, Z.Sujkowski, I.F. W.Jansen, W.J.Ockels, M.J.A.de Voigt, Cross sections of the (α,xn) reaction on ^{154}Gd and ^{160}Gd nuclei in the Eα = 47-130 MeV energy range, in: Annu. 28. All-Union Conf. Nucl. Spectrosc. Nucl. Struct. Alma-Ata, 1978: pp. 2369–2372.

[8] A.K.M.R. Rahman, A. Awal, Production of ^{149}Tb, ^{152}Tb, ^{155}Tb and ^{161}Tb from gadolinium using different light-particle beams, J. Radioanal. Nucl. Chem. 323 (2020) 731–740. https://doi.org/10.1007/s10967-019-06973-0.

[9] A.J. Koning, D. Rochman, J.C. Sublet, N. Dzysiuk, M. Fleming, S. van der Marck, TENDL: Complete Nuclear Data Library for Innovative Nuclear Science and Technology, Nucl. Data Sheets. 155 (2019) 1–55. https://doi.org/10.1016/j.nds.2019.01.002.

[10] K.Y. T. Watanabe, M. Fujimaki, N.Fukunishi, H. Imao, O.Kamigaito, M. Kase, M.Komiyama, N. Sakamoto, K.Suda, M.Wakasugi, Beam energy and longitudinal beam profile measurement system at the RIBF, Proc. 5th Int. Part. Accel. Conf. (IPAC 2014). (2014) 3566–3568.

[11] J.F. Ziegler, J.P. Biersack, M.D. Ziegler, SRIM: the Stopping and Range of Ions in Matter, (2008). http://www.srim.org.

[12] National Nuclear Data Center, Nuclear structure and decay data on-line library, Nudat 2.8, (2018). https://www.nndc.bnl.gov/nudat2/.

[13] S.Y.F. Chu, L.P. Ekström, The Lund/LBNL Nuclear Data Search, (1999). http://nucleardata.nuclear.lu.se/toi/.

[14] International Atomic Energy Agency, LiveChart of Nuclides, (2009). https://www-nds.iaea.org/livechart/.

[15] B. Pritychenko, A. Sonzogni, Q-value Calculator (QCalc), (2003). http://www.nndc.bnl.gov/qcalc/.

[16] Z.B. Alfassi, E. Persico, F. Groppi, M.L. Bonardi, On the photon self-absorption correction for thin-target-yields vs . thick-target-yields in radionuclide production, Appl. Radiat. Isot. 67 (2009) 240–242. https://doi.org/10.1016/j.apradiso.2008.10.004.

[17] Photon Interaction Database, National Institute of Standards and Technology, (2004). https://physics.nist.gov/PhysRefData/XrayMassCoef/tab3.html.

[18] A. Hermanne, A. V. Ignatyuk, R. Capote, B. V. Carlson, J.W. Engle, M.A. Kellett, T. Kibédi, G. Kim, F.G. Kondev, M. Hussain, O. Lebeda, A. Luca, Y. Nagai, H. Naik, A.L. Nichols, F.M. Nortier, S. V. Suryanarayana, S. Takács, F.T. Tárkányi, M. Verpelli, Reference Cross Sections for Charged-particle Monitor Reactions, Nucl. Data Sheets. 148 (2018) 338–382. https://doi.org/10.1016/j.nds.2018.02.009.